Submarine gas seepage in a mixed contractional and shear deformation regime: Cases from the Hikurangi oblique-subduction margin

Andreia Plaza-Faverola
GNS Science, Avalon, Lower Hutt 5010, New Zealand

*Department of Geology, University of Tromsoe, Dramsveien 201, Tromsø 9037, Norway
(andreia.a.faverola@uit.no)*

Ingo Pecher
GNS Science, Avalon, Lower Hutt, New Zealand

School of Environment, The University of Auckland, Auckland, New Zealand

Gareth Crutchley
GNS Science, Avalon, Lower Hutt, New Zealand

GEOMAR, Helmholtz Centre for Ocean Research Kiel, Kiel, Germany

Philip M. Barnes
National Institute of Water & Atmospheric Research, Wellington, New Zealand

Stefan Bünz
Center for Arctic Gas Hydrate, Environment and Climate, University of Tromsoe, Norway

Thomas Golding
GNS Science, Avalon, Lower Hutt, New Zealand

Shell, Perth, WA, Australia

Dirk Klaeschen, Cord Papenberg, and Joerg Bialas
GEOMAR, Helmholtz Centre for Ocean Research Kiel, Kiel, Germany

[1] Gas seepage from marine sediments has implications for understanding feedbacks between the global carbon reservoir, seabed ecology, and climate change. Although the relationship between hydrates, gas chimneys, and seafloor seepage is well established, the nature of fluid sources and plumbing mechanisms controlling fluid escape into the hydrate zone and up to the seafloor remain one of the least understood components of fluid migration systems. In this study, we present the analysis of new three-dimensional high-resolution seismic data acquired to investigate fluid migration systems sustaining active seafloor seepage at Omakere Ridge, on the Hikurangi subduction margin, New Zealand. The analysis reveals at high resolution, complex overprinting fault structures (i.e., protothrusts, normal faults from flexural extension, and shallow (<1 km) arrays of oblique shear structures) implicated in fluid migration within the gas hydrate stability zone in an area of 2×7 km. In addition to fluid migration systems sustaining seafloor seepage on both sides of a central thrust fault, the data show seismic evidence for subseafloor gas-rich fluid accumulation associated with proto-thrusts and extensional faults. In these latter systems

fluid pressure dissipation through time has been favored, hindering the development of gas chimneys. We discuss the elements of the distinct fluid migration systems and the influence that a complex partitioning of stress may have on the evolution of fluid flow systems in active subduction margins.

1. Introduction

[2] Seafloor gas seepage, often associated with gas hydrate accumulations, has gained significant research attention over the last few decades. This is because of the large unconventional carbon reservoir that gas hydrates represent, and the potential for large amounts of greenhouse gases to escape from marine sediments, which may have influenced glacial-interglacial changes and the Earth's global climate [e.g., *MacDonald*, 1990; *Kvenvolden*, 2002; *Denman et al.*, 2007; *Etiope*, 2009]. Noteworthy natural carbon sources to the atmosphere include microbial oxidation of organic matter [e.g., *Kurtz et al.*, 2003], hydrate dissociation [e.g., *Dickens et al.*, 1995; *Kennett et al.*, 2003], thermal decomposition of organic matter and volcanic outgassing [e.g., *Kroeger et al.*, 2011; *Svensen*, 2012], and degassing of shallow sediments through faults and fractures [e.g., *Etiope et al.*, 2008; *Milkov et al.*, 2003]. Methane gas (CH_4) from geological sources (thermogenic, microbial, and geothermal methane) is estimated to account for at least 10% of the atmospheric methane budget, making geological sources potentially the third most important methane source after wetlands and anthropogenic emissions [*Etiope et al.*, 2008].

[3] Microbial and thermogenic CH_4 in marine sediments is transported to the seafloor through permeable pathways. The migration of overpressurized fluids from shallow reservoirs to the seafloor leads to deformation of the sediments and development of gas chimneys and mud volcanoes, also known as plumbing systems [*Talukder*, 2012 and references therein]. The internal structure and driving mechanisms of these plumbing systems remain the least understood components of fluid flow systems [e.g., *Judd and Hovland*, 2007; *Anka et al.*, 2012]. One key factor in understanding their development is the mechanical deformation of sediments determined by the stress history [*Talukder*, 2012]. Many cases of fluid migration through permeable polygonal, extensional, or thrust faults have been reported worldwide [e.g., *Hyndman and Davis*, 1992; *Berndt et al.*, 2003; *Gay et al.*, 2007; *Hustoft et al.*, 2007; *Crutchley et al.*, 2011]. Other studies have shown manifestations of fluid flow though mobilized sediments [e.g., *Cartwright et al.*, 2007], and a few studies have explored plumbing mechanisms in response to shear failure [*Cartwright*, 2011; *Zühlsdorff and Spiess*, 2004].

[4] On the Hikurangi subduction margin, New Zealand, numerous active fluid seeps occur on the crests of major ridges [*Barnes et al.*, 2010; *Greinert et al.*, 2010]. At Omakere Ridge, (Figure 1), seafloor methane seep sites have been documented and characterized in terms of their morphology and relative level of activity [*Jones et al.*, 2010; *Golding*, 2012]. Gas hydrates have been sampled within the upper meter of sediments at seep sites [*Bialas et al.*, 2007]. A seismic experiment was carried out in 2011 to determine the three-
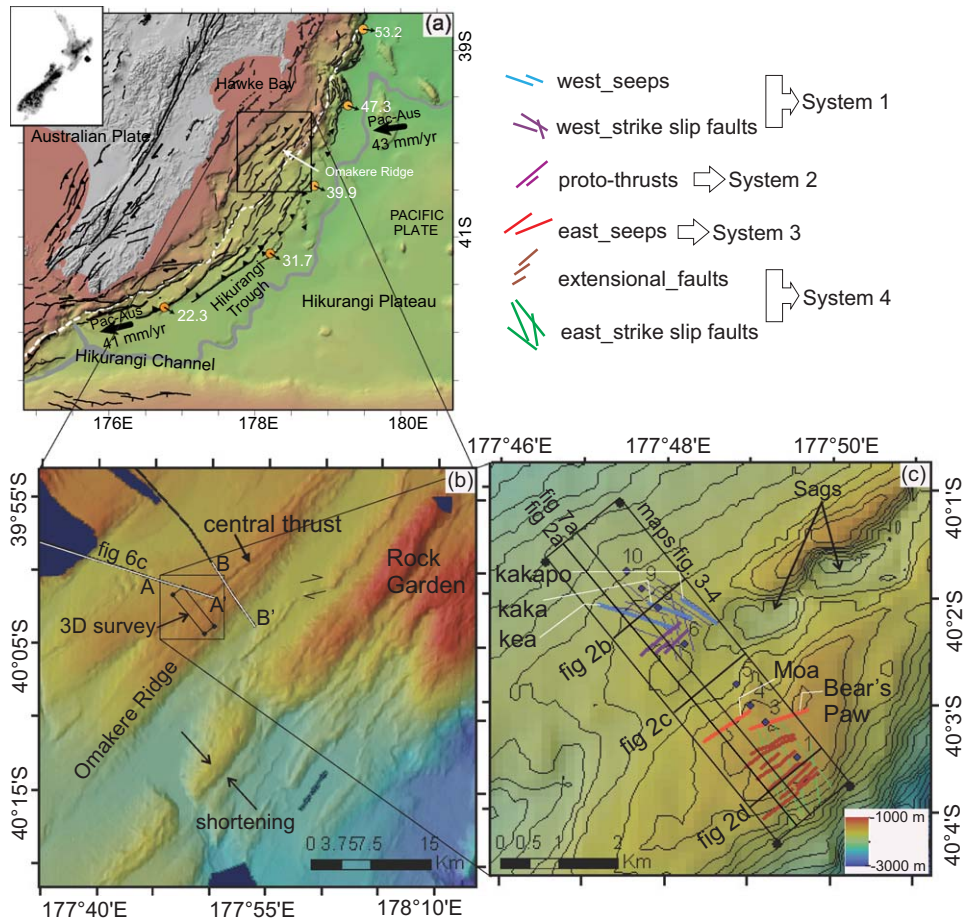
Figure 1. (a) Bathymetry map showing the location of Omakere Ridge at the Hikurangi margin. Geological structures are from *Barnes et al.* [2010]; Pacific-Australian plate motion vectors from *Beavan et al.* [2002]; modeled relative motion between the East Coast Hikurangi crustal block and the subducting Pacific Plate (orange dots with vectors) from *Wallace et al.* [2004]. (b) Location of the 3-D survey with respect to the structural setting, and regional lines showing BSRs in Figure 6. (c) Magnified display of the study area showing the orientation vectors of faults and seeps. The numbers correspond to ocean bottom seismic (OBS) stations. The legend (above) indicates main features of the four fluid migration systems discussed in the paper.

dimensional structure of the plumbing systems underlying these seeps [*Bialas*, 2011]. The experiment consisted of a high-resolution 3-D-seismic survey using the P-Cable seismic imaging apparatus [*Planke and Berndt*, 2003] and an array of 10 ocean bottom seismometers (OBSs). This paper presents the subsurface structural elements of different fluid migration systems, with and without associated present-day seafloor seepage, and proposes a complex deformation regime under the mixed influence of shear and compression.

2. Tectonic and Stratigraphic Settings

[5] New Zealand's North Island is bounded by the Hikurangi-Trough, where the Pacific Plate sub-

ducts westward and obliquely beneath the Australian Plate at about 40–50 mm/yr [*Beavan et al.*, 2002]. The tectonic style of the Hikurangi margin varies depending on the thickness and roughness of the underthrusting crust, obliquity of convergence, and thickness of subducting sediments [e.g., *Lewis and Pettinga*, 1993; *Collot et al.*, 1996; *Barnes et al.*, 2010]. Toward the northern Hikurangi margin, thick oceanic crust of the Pacific Plate is subducting obliquely at ~50 mm/yr, with part of the margin-parallel motion being accommodated by strike-slip faulting [*Berryman and Beanland*, 1988; *Collot et al.*, 1996]. The relative plate motion is progressively more oblique southward, where subduction eventually makes the transition to a continental transform boundary [*Wallace et al.*, 2012].

[6] Toward the NW, the inner Hikurangi margin is underlain by imbricated Cretaceous and Cenozoic presubduction sequences and a cover of syn-subduction Miocene to recent sediments. Toward the SE, the outer margin is composed of a late Cenozoic frontal accretionary wedge [*Cole and Lewis*, 1981; *Davey et al.*, 1986; *Lewis and Pettinga*, 1993; *Barnes et al.*, 2010].

[7] Omakere Ridge lies in a region of the central Hikurangi margin where the plate convergence vector lies 40–50° oblique to the plate boundary. Whilst dextral faulting has been interpreted more than 70 km westward [*Haines and Darby*, 1987; *Cashman et al.*, 1992], active dextral faults have not been recognized offshore in the upper slope region of southern Hawke's Bay. This area has previously been interpreted as largely contractional [*Lewis and Pettinga*, 1993; *Barnes et al.*, 2010; *Paquet et al.*, 2011].

[8] Omakere Ridge lies at about 1200 m water depth (Figure 1b). The easternmost flank of the ridge is underlain by an active thrust and deeper inactive thrust imbricates [*Barnes et al.*, 2010]. A second active thrust splay reaches the seafloor along the middle of the ridge (referred to as "central thrust" (CT) in Figure 1b). The ridge is underlain by a wedge of Cretaceous and Paleogene rocks and a Miocene to Recent cover sequence. Active seeps at Omakere Ridge lie in the hanging wall of both the CT and a deeper thrust fault emerging at the seafloor at the base of the eastern flank (forelimb) of the ridge.

2.1. Morphology of Seep Sites at Omakere Ridge: Background

[9] Methane seep sites at Omakere Ridge are recognized as high backscatter regions and positive relief structures on sidescan sonar and multibeam swath bathymetry [*Greinert et al.*, 2010; *Jones et al.*, 2010; *Golding*, 2012]. Five seep sites are within the 3-D-seismic survey: Kea, Kaka, Kakapo, Moa, and Bear's Paw (Figure 1). The activity of these seeps has been inferred based on the abundance of chemosynthetic fauna and methane concentrations in the water column [*Faure et al.*, 2010; *Jones et al.*, 2010]. Bear's Paw is identified as the most active seep site, followed by Kea [*Jones et al.*, 2010]. Gas hydrates were recovered in sub-horizontal layers at ∼1 m below the Bear's Paw site [*Bialas et al.*, 2007]. Moa comprises an extinct part, characterized by a high relief authigenic carbonate build-up and associated cold-water corals, and a low relief structure where anomalous meth-

ane concentration in the water column and living chemosynthetic fauna indicate present-day activity. Kaka and Kakapo are also associated with live chemosynthetic fauna and are thus believed to be currently active [*Jones et al.*, 2010].

3. Methods

[10] A high-resolution 3-D-seismic survey was acquired using the P-Cable seismic imaging tool during cruise SO214 aboard R/V SONNE [*Bialas*, 2011]. For this survey, the P-Cable system was used in a configuration with 16 streamers attached at 10 m separation along the cross-cable. The source consisted of a 4.2 L GI-gun deployed at 2 m water depth with a shot interval of 6 s. The 3-D survey covered an area of ∼2 × 7 km oriented perpendicular to the axis of Omakere Ridge (Figure 1). Data were recorded at a sampling rate of 0.25 ms and were resampled to 1 ms. Processing of the data included CDP binning at 6.25 m bin size, band pass filtering, deconvolution to attenuate seafloor ghosts, tide and residual static corrections, poststack interpolation to fill in data gaps, and 3-D Kirchhoff time migration. The vertical resolution of the data is ∼6.25 m, taken as $\lambda/4$ at 1500 m/s with a dominant frequency of 60 Hz. The lateral resolution is ∼6.25 m—the CDP spacing in the migrated 3-D volume used for interpretation.

[11] Data were converted to depth using an average velocity function from OBSs that recorded data along the inline direction at the center of the 3-D survey (Figure 1). OBS receiver gathers were redatumed to sealevel followed by conventional semblance analysis [e.g., *Bünz et al.*, 2005; *Netzeband et al.*, 2005]. The resulting averaged 1-D velocity function enabled us to make a good approximation of the depth of reflections in the volume, appropriate for the structural interpretations made in this paper. More detailed velocity analysis from OBS data is on-going and will be presented elsewhere.

[12] Root-mean-square (RMS) amplitudes and trace coherency were calculated along surfaces at different depths within the seismic volume (Figures 3 and 4) to investigate relationships between structural features and fluid migration indicators appearing at different stratigraphic levels. The location of surfaces within the volume is presented in Figure 2. Seafloor seep sites and gas accumulations, as well as chimneys, manifest themselves strongly in RMS amplitude maps (i.e., as high and low RMS amplitudes, respectively), while faults, fractures, and other structural features characterized
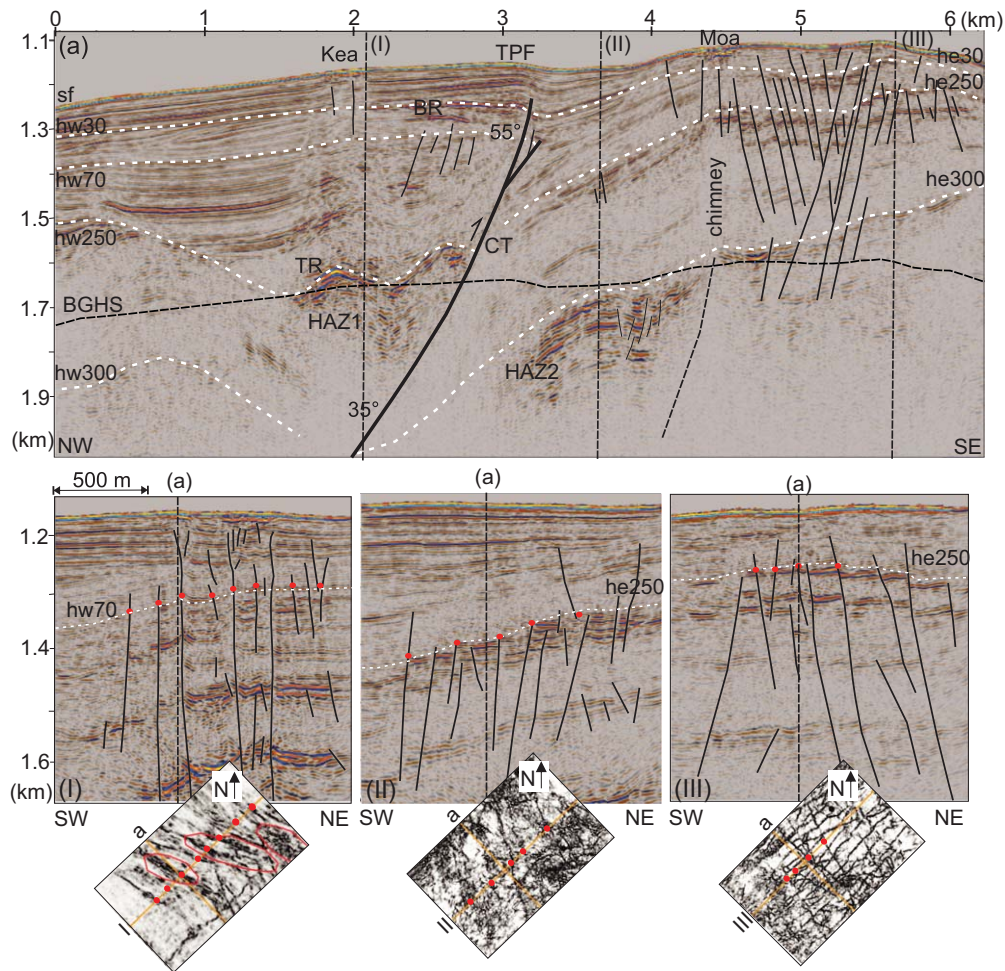
Figure 2. Seismic profile scaled to depth (a) showing main structural interpretation and the location of interfaces where attributes maps have been extracted. TPF = thrust propagation fold; CT = central thrust; BR = bright reflection; TR = top of reservoir; HAZ = high-amplitude zone; BGHS = base of the hydrate stability zone (projected from previous studies). The panels (I–III) show seismic character of faults oriented obliquely with respect to the TPF. Insets show the oblique faults along cross-sections I–III on coherence maps at the depth of hw70 and he250 (see Figure 4 for complete map). Yellow lines indicate orientation of seismic lines. Red polygons indicate location of seeps Kea, Kaka, and Kakapo. Red dots match faults interpreted on the cross-lines. See Figure 1c for location of the profiles.

by dipping flanks are illuminated best in coherence maps. Trace coherency (i.e., quantification of local waveform similarity using dip and azimuth) was calculated using a vertical aperture of 30 ms to highlight high-angle, vertically persistent faults and fractures. A rectangular half aperture of 1 trace was used (i.e., 1 trace on each side of the central trace was used for semblance calculation). RMS amplitudes were calculated within windows of 40–100 ms centered at specific surfaces.

[13] Our results and discussion are based on five main attribute maps. From top to bottom, the maps are as follow: sf (Figure 3a) shows RMS amplitudes extracted along the seafloor; hw30-he30

(Figure 3b) shows coherency extracted along unconformities at the base of a sedimentary succession where fault overprinting is not observed; hw70-he250 (Figure 3c) present coherency along the interfaces that best show fault overprinting on both sides of CT; hw250-TR-he250 (Figure 3d) shows RMS amplitudes along an envelope of high-amplitude reflections associated with major stratigraphic unconformities on both sides of CT; and hw300-he300 (Figure 3e) shows RMS amplitudes along the top reflection of a second high-amplitude package, mainly present on the footwall of CT. The maps present attributes extracted along interfaces that show unique features at specific depths, which do not necessarily represent same
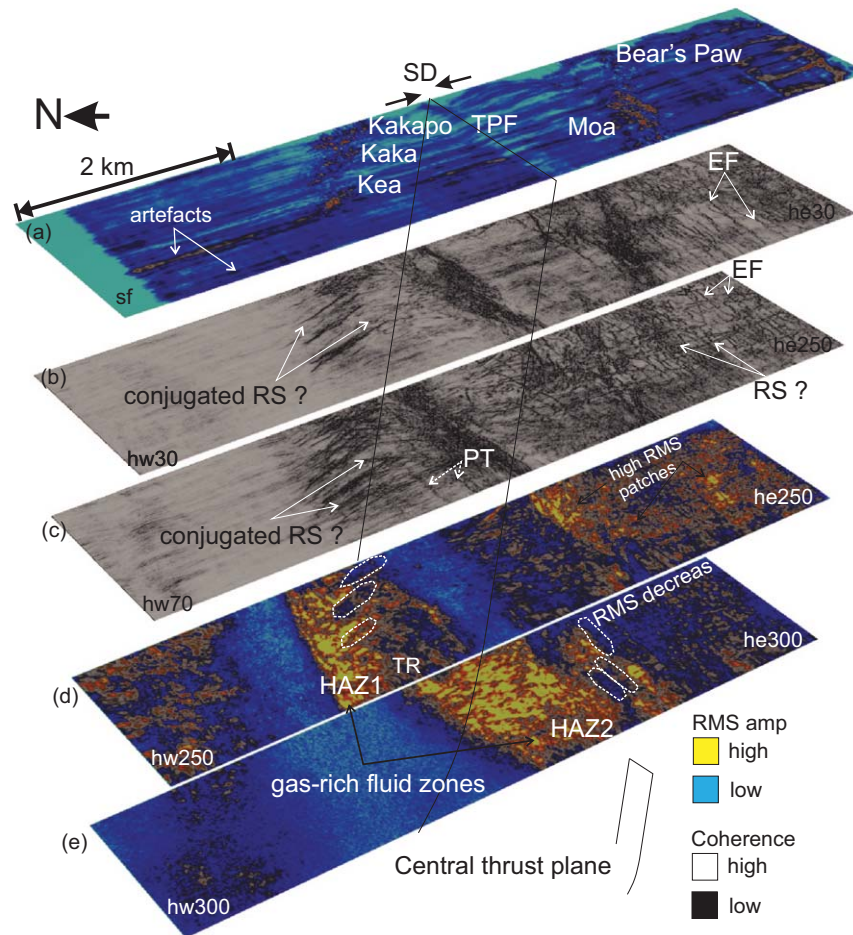
Figure 3. Attribute maps extracted along key interfaces showing spatial relationship between faults and fluid flow-related features (see Figure 2 for vertical location). Interfaces on both sides of the central thrust fault plane do not necessarily represent same stratigraphic levels. The view of the maps is from the North-West (Figure 1). See Figure 4 to obtain the azimuths of faults and seeps. SD = shortening direction; (a) RMS amplitude map extracted along the seafloor. All the seeps except Bear's Paw appear as high-RMS amplitudes. TPF = thrust propagation fold; (b) Coherency map centered at hw30 and he30 to the west and east of the TPF, respectively. EF = extensional faults, RS = Riedel shears; (c) Coherence map extracted along hw70 (west) and he250 (east), displayed together to show continuity of appearing oblique faults on both sides of the TPF. PT = proto-thrusts; (d) RMS amplitude map extracted along an interface composed by hw250, TR (top reservoir) and he250. A high-amplitude zone (HAZ) underlies seeps Kea, Kaka, and Kakapo; (e) RMS amplitude map along hw300 and he300. A second HAZ developed associated with a blind thrust fault to the west of Moa and Bear's Paw seeps. Dash-white lines indicate seep projection on maps (d) and (e). Notice that chimney conduits are characterized by low-RMS amplitudes.

chronological events on both sides of CT (presented together for visualization purposes), since stratigraphic constraints are not available in the area. We used different names for interfaces interpreted on both sides of CT to reflect this unknown chrono-stratigraphy within the ridge (Figure 2).

[14] Fault planes were extracted by auto-detection of connectivity within laterally interrupted reflections using available software (Petrel®). Rose diagrams with the azimuths of extracted fault planes

were used for analysis of fault orientation with respect to the orientation of seafloor gas seep morphologies. Seep site morphology and fault orientations were compared against geological features observed in the bathymetry (Figure 1).

4. Results

[15] Five high-resolution seismic maps extracted along key horizons from the 3-D survey (i.e.,
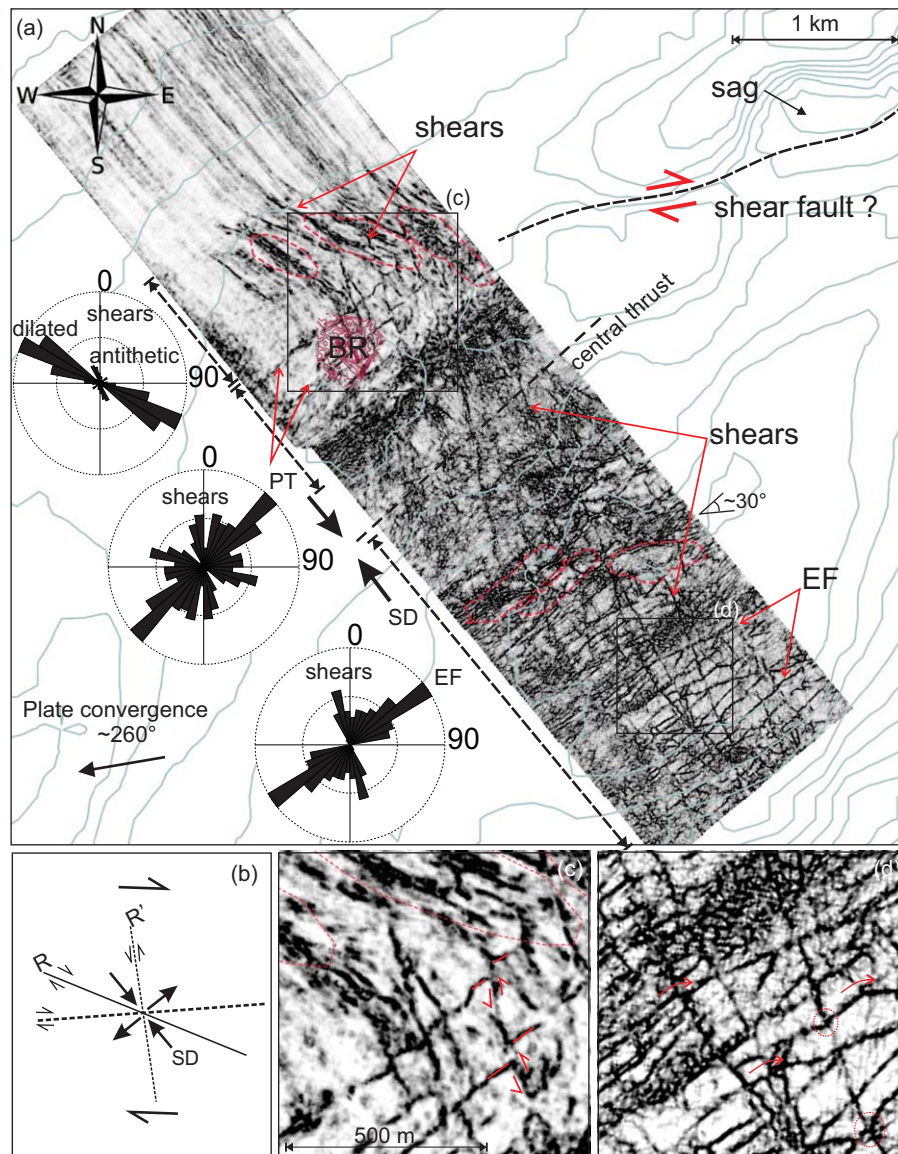
Figure 4. (a) Coherency map along hw70 and he250 (see Figure 2 for location) showing the orientation of overprinting faults (rose diagrams) on both sides of the central thrust. Plate convergence vector is from *Beavan et al*. [2002]. PT = proto-thrusts, EF = extensional faults, SD = shortening direction, CT indicates projection of the fault plain on the bathymetry. Seeps (dashes red lines) as well as the contours of the bright spot (BR) are projected. (b) The vector diagram shows a simple shear model for comparison (after *Sylvester* [1988]). (c) and (d) Magnified displays of conjugated shears showing indications of potential strike-slip displacement manifested in cross-cutting faults and clockwise rotation due to possible dextral lateral shear deformation.

orthogonal to the axis of Omakere Ridge; Figure 1) show the interconnection between gas-rich fluid accumulations and the structural elements of fluid migration systems within the upper 600 m of sediments at Omakere Ridge.

[16] Figure 3 shows through a series of composed maps, the vertical relationship between faults, seeps, and chimneys and the distribution of gas-rich fluid accumulations. New overprinting faults and fluid migration related features appear consec-

utively in deeper maps on both sides of the central thrust fault. The orientations of different features and their spatial distribution with respect to regional structures are better represented in Figures 1 and 4.

4.1. The Central Thrust Fault and Associated Deformation Structures

[17] The central thrust shows a dip increase from ∼35° at a depth > 1700 m to ∼55° within the
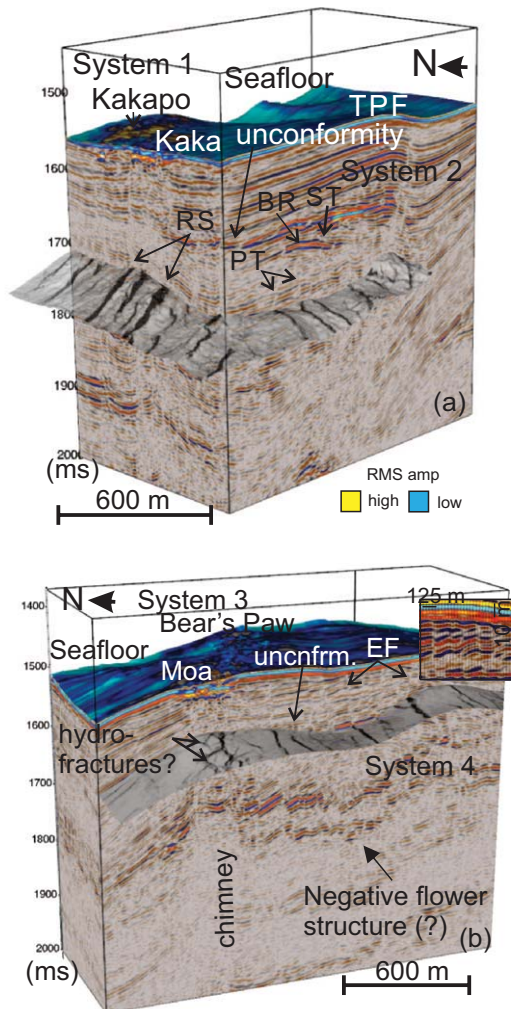
Figure 5. (a) 3-D view of System 1 and System 2 showing verticality of conjugated faults determining orientation of seeps Kea, Kaka, and Kakapo, seismic expression of proto-thrust (PT) and stratigraphic truncation (ST) at overlying bright reflection (BR). TPF = thrust propagation fold; (b) 3-D view of Systems 3 and System 4 showing extensional faults (EF) at the collapsed ridge crest. The inset is a magnified view of the normal fault offsets. Deeper maps show faults extracted automatically using the Ant-Tracking algorithm (Petrel®).

upper 100 m of sediments, and it has an associated thrust propagation fold (TPF) (Figures 2a and 5a). The TPF extends toward the seafloor with a strike of ~035°.

[18] A set of elongated en echelon depressions or sags are located along the axis of the TPF, ~2 km north of the 3-D seismic volume (Figure 1c). The sags are >800 m in width and have their long axis oriented ENE-WSW, with azimuths between 060 and 090° (Figure 1c). In vertical seismic profiles, they appear as grabens with shallow-penetrating

(500 ms) extensional faults at the flanks (Figure 6).

4.2. Faults and Seepage on the Hanging Wall of the Central Thrust Fault

[19] Seafloor seepage expressions on the hanging wall of the CT (Kea, Kaka, and Kakapo) [e.g., *Golding*, 2012] are oriented NW-SE at azimuths of ~290° (Figure 4). Coherency maps show arrays of closely-spaced (i.e., 30–90 m separation) parallel and near-parallel faults oriented NW-SE (oblique to the CT) underlying seep sites and mimicking their azimuths (Figures 3 and 4). Each seafloor seep site appears to be sustained by more than one thin conduit. Faults oriented NNW-SSE emerge toward the east of the seeping area with azimuths around 310–330° (Figures 1, 3, and 4). In seismic profiles, these pseudoconjugated faults are subvertical (Figures 2b and 5a). While some of them appear to be associated with gentle, normal (i.e., extensional) vertical displacement of reflections, others do not show evident normal or reverse (i.e., compressional) vertical displacement (Figure 2b). They are restricted to an area of ~1.5 km from the CT.

[20] The lateral extent of faulting and seafloor seepage (i.e., ~1 km along the ship track) coincides with the extent and morphology of an underlying ~100 m thick zone of enhanced amplitudes (HAZ1; Figure 2). This zone of enhanced amplitudes is restricted to a pair of small folds bounded to the SE by the CT and to the NW by a major stratigraphic unconformity (Figure 2a). RMS amplitude maps show that the highest amplitudes occur at the crest of the westernmost fold (Figure 3d). The anomalous amplitude distribution characterizing HAZ1 provide evidence for a structurally controlled gas-rich fluid accumulation zone [e.g., *Løseth et al.*, 2009; *Berndt et al.*, 2012]. The top reflection of this gas zone is at a depth of ~500 mbsf (Figures 2a and 3d). Here, flat bright reflections cross-cut the stratigraphy (Figures 2 and 7) possibly indicating a local bottom simulating reflector (BSR). Contours at this depth show elongated structural highs coinciding with the highest RMS amplitudes in the maps (Figure 3d). The structural highs also match the orientation and distribution of seafloor seep sites (Figure 7b).

[21] Vertical zones of seismic blanking mark the extent of the seepage systems (i.e., gas chimneys) underlying seep sites Kea, Kaka, and Kakapo (Figure 2). Blanking is weaker above an unconformity at ~100 mbsf (i.e., surface hw30, Figure 2a) and
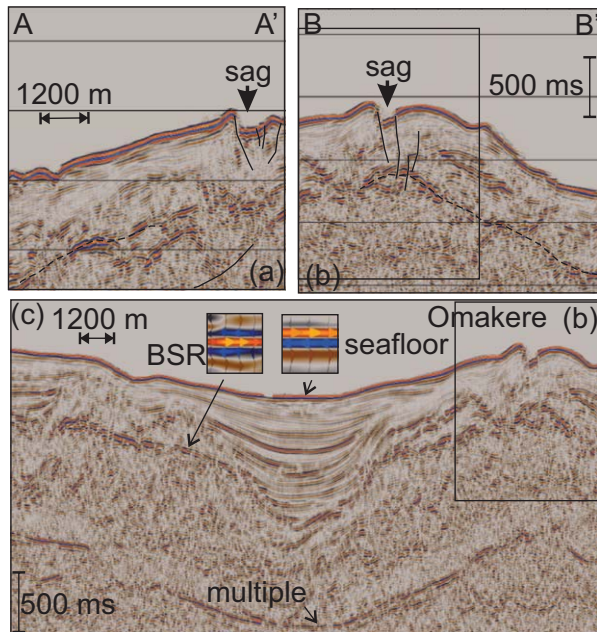
Figure 6. Regional lines showing seismic character of sag-like structures along the central thrust (see Figure 1 for location). The profile in Figure 6c shows the westward continuation of Figure 6b where a clear BSR exists. Insets show polarity of BSR with respect to the seafloor. The BSR from Figure 6c is projected as dashed line on Figures 6a and 6b where the BSR is less clear.

does not extend deeper than the gas zone (HAZ1). Here, the term "chimney" refers to an aggregation of closely spaced parallel conduits. The chimneys are easily recognized on RMS amplitude maps as elliptical zones of low RMS amplitudes surrounded by high RMS amplitudes (Figure 3d). Low RMS amplitude patches are ~700 × 200 m beneath Kaka and Kakapo and ~400 × 150 m beneath Kea (Figure 3d). Contrary to some margins where cylindrical or near-cylindrical chimneys underlie the seeps [e.g., *Pilcher and Argent*, 2007; *Hustoft et al.*, 2010], chimneys at Omakere Ridge are observed as strongly elliptical to elongated low RMS amplitude anomalies (Figures 3d and 3e).

4.3. Proto-Thrusts and Associated Gas-Rich Fluid Accumulations

[22] In the hanging wall of CT, south of seep sites Kea, Kaka, and Kakapo, a set of proto-thrusts (i.e., subtle reverse faulting) are developed, striking ~045°, subparallel to the CT (Figure 4). The proto-thrusts are 70–100 m apart, restricted to sediments above the easternmost fold of strata containing HAZ1 (Figure 2). They are overprinted

by the high-angle NNW-SSE component of the shear faults array associated with Kea, Kakapo, and Kaka seeps. Their lateral extent coincides with a region of diminished RMS amplitudes at the top of HAZ1 (Figure 3d). No seafloor seep sites are associated with the proto-thrusts (Figures 2a and 3c). Instead, a ~400 m diameter bright reflection (BR) is mapped at the depth of an unconformity right at the upper termination of the proto-thrusts (i.e., at the hw30 horizon; Figures 4, 5, and 7). The wave-form polarity of BR appears to be normal (i.e., the same as that of the seafloor reflection) around the periphery of the reflection, but reversed toward the center of it, where the highest RMS amplitudes occur (Figure 7b). BR is slightly convex-upward, with a gentle positive doming of ~10 m (Figure 7a) and it has the characteristics of a "bright spot", commonly used as indicators of gas caps in the sediments [e.g., *Løseth et al.*, 2009]. Smaller reverse-polarity bright reflections confined to sedimentary layers displaced by the proto-thrusts at different stratigraphic levels below BR (Figure 7a), indicate additional gas-rich fluid accumulations.

4.4. Ridge-Parallel Seepage and Fault Overprinting East of the Central Thrust

[23] To the east of CT the Omakere Ridge is characterized by a bathymetric crestal depression or graben (Figures 2a and 5b). Coherency maps at ~90 mbsf show parallel, closely spaced (~90 m), also NE-SW trending (parallel to CT) extensional faults concentrated in the graben (Figure 5b). In vertical profiles, these faults show normal displacement with offsets <10 m in the upper 100 m of sediments, increasing to larger offsets deeper in the sedimentary sequence (Figures 2a and 5b). Seafloor seep sites have been observed exclusively on the westernmost flank of the graben. These seep sites (Moa and Bear's Paw) are oriented NE-SW, at a high angle to the NW-SE oriented Kea, Kaka, and Kakapo seep sites to the west of CT (Figure 3).

[24] A deeper and apparently older set of curvilinear faults, striking NNW-SSE (Figures 3c and 4), is evident at a high angle to the extensional faults at ~1350 m (map extracted along horizon he250; Figure 2a). The strike of these faults varies from ~360° in the north of the volume to ~320° in the south of the volume (Figure 4). These faults have comparable orientations to the NNW-SSE striking shear faults west of the CT (Figures 3c and 4), but are developed in the sequence mainly
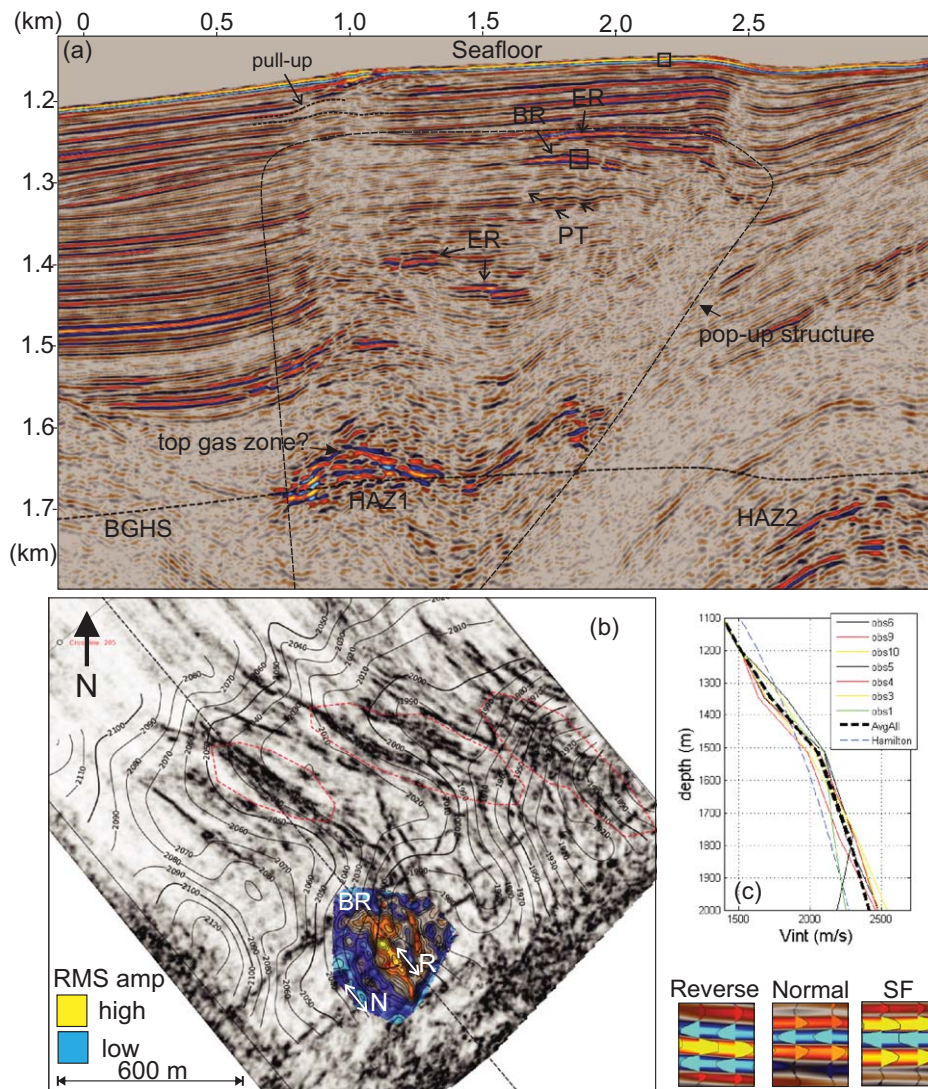
Figure 7.   (a) Seismic section scaled to depth. The squares indicate location of wiggle panels in Figure 7b. BR = bright reflection, HAZ = high-amplitude zone, ER = enhanced reflections. BGHS is the BSR-based regional base of gas hydrate stability projected from previous studies; (b) Coherency map with contours from top of HAZ1 and bright reflection (BR) as well as seeps Kea, Kaka, and Kakapo are projected. N indicates normal and R reverse polarity with respect to the seafloor (SF) polarity. The dash line indicates location of profile in Figure 7a. (c) Averaged OBS-derived P-wave velocity (Vp) curve used for depth conversion of our data compared against the *Hamilton* [1978] curve for normally compacted sediments.

beneath horizon he250, and in contrast to those west of the CT, are not active. They appear to be overprinted by the ridge-parallel extensional array associated with the axial bathymetric graben. Toward the western flank of the graben these curvi-linear structures are less overprinted by overlying extensional faults, showing gentle normal displacement to no displacement (Figures 2c and 2d).

[25] Seafloor seep sites Moa and Bear's Pau are aligned along the same dominant underlying structure at the western flank of the graben. The seeps

have slightly different orientation: Moa aligns NE-SW, and Bear's Paw ENE-WSW. These are approximately parallel to the CT and TPF, with Bear's Paw locally rotated eastward with respect to Moa (Figure 4).

[26] The chimneys underlying Moa and Bear's Paw are recognized as low RMS amplitude anomalies with comparable dimensions to chimneys to the west of the CT (Figure 3e). The seismic blanking is less pronounced beneath Bear's Paw. In general, blanking is more pronounced beneath he250 and chaotic reflections dominate

Table 1. Structural Summary[a]

	Outer Wedge[a]		Central Thrust (CT)		Protothrusts		Active-Conjugated Shears		Ridge Parallel Normal Faults		Inactive Shears	
	Strike	Dip	Strike	Dip	Strike	Dip	Strike	Dip	Strike	Dip	Strike	Dip
	125 (305) Likely to be σ1		045 (225)	35–55		>55	110 (290) NW; 130–150 (310–330) SE	80–90	050 (230)	>55	180 (360) N; 140 (320) S	80–90
Associated fluid migration features			Conduits for deep fluid sources		Bright reflection (BR): subseafloor fluid accumulation (System 2)	Kea, Kaka, and Kakapo seeps and chimneys (System 1)	Moa and Bear's Paw seeps and chimneys (System 3)	High RMS amplitude patches: subseafloor fluid accumulations (System 4)				
Interpretation			Active thrust imbricate and TPF		Inactive; likely formed in association with CT	Several possible interpretations (see section 5.1.)	Active flexural extension of ridge crest overprints inactive conjugate shears	Several possible interpretations, (see section 5.1.)				

[a]*Wallace et al.* [2004].

above an unconformity that marks the depth limit at which only the NE-SW striking extensional faults are observed in the maps (Figures 2d and 3b).

[27] A $\sim$200 m thick interval characterized by high RMS amplitudes (HAZ2; Figure 3e) indicates a second gas-rich fluid accumulation zone (similar to HAZ1; Figure 2a). This gas-rich zone is restricted to folded strata that are truncated to the SE by an inactive thrust imbricate [*Barnes et al.*, 2010] buried at a depth of $\sim$1.7 km to the east of the CT (Figures 2a and 3e). The top reflection of HAZ2 is at 450–520 mbsf (i.e., deepening southward within the seismic survey). Seafloor seepage does not occur directly above HAZ2, but the distribution and orientation of seep sites coincides with the vertical projection of the buried thrust tip (Figures 2 and 3e). High RMS amplitudes are not present eastward of the buried thrust fault along he300 (Figure 3e). However, smaller high RMS amplitude patches, bounded by the shallow overprinting faults (Figure 3d), reappear at shallower depths (e.g., at the depth of horizon he250; Figure 2a).

5. Discussion

5.1. Seafloor Seepage and Its Relation to Shear, Shortening, and Stress

[28] The difference in orientation of seep sites on both sides of the CT reveals fluid migration responses to local compressional, shear, and extensional deformation, as well as a polyphase deformational history of Omakere Ridge. Notwithstanding that the regional stress state in accretionary wedges may switch dramatically, from compressional to extensional, in association with mega-thrust earthquake cycles [e.g., *Sibson*, 2013], it can be thus expected that the growth of major active forearc thrust faults and folds (striking $\sim 035°$) in the study region, reflects the average orientation of the maximum compressive stress (σ_1) to be $\sim 305°$. In the hypothetical case that Omakere Ridge lies in a purely compressive stress regime [*Wallace et al.*, 2004], the contemporary shortening direction can be assumed to be oriented NW-SE, parallel to σ_1 (Figure 4 and Table 1).

[29] To the west of the CT, the morphology of Kea, Kaka, and Kakapo seep sites reflects the orientation of shear faults developed oblique to the principal shortening direction (i.e., indicated by

the thrusts and folds), while the morphology of Moa and Bears Paw seeps reflects the orientation of thrust faults and/or extensional faults (Figure 4). We interpret the array of NE-SW oriented extensional faults at the crest of the ridge east of Moa seep (Figure 5b) likely results from flexural extension in the upper stratigraphic level of the Omakere Ridge anticline. Extensional collapse and increase of the fault offsets with depth (Figure 5b) indicates growth of these faults over a substantial (c. $10^5 - 10^6$ years) stratigraphic interval [e.g., *Barnes et al.*, 2010].

[30] The conjugate oblique faults (290°–330°) on both sides of the active CT (Figure 4 and Table 1) have not previously been observed in the Hikurangi margin, and are a surprising discovery of this survey. They appear from apparent lateral offsets in the coherency maps, to be shear faults (Figure 4). There are several possible interpretations for the development of these oblique shear faults. They may have initiated as extension or conjugate shear joints related to the development of Omakere Ridge anticline. Such joints are common in fold systems and reflect extension parallel to the fold axis [e.g., *Sylvester*, 1988]. However, although shear faults are observed on both sides of the CT (Figure 4a), only those shears in the hanging wall of the CT remain active and show two conjugated components (i.e., shears at the footwall are not observed above horizon he250 (Figure 3c) and appear only oriented NNW-SSE (Figure 4). This observation suggests that shear faults west and east of CT may have developed somewhat independently and leads to alternative interpretations.

[31] If it is assumed that deformation has been primarily compressional [e.g., *Barnes et al.*, 2002; *Wallace et al.*, 2004], and approximately normal to the active CT and TPF, the conjugate shear faults could be explained with a Coulomb-Anderson model (pure shear) involving complex stress perturbations in the shallow part of the ridge. The maximum compressive stress may be approximately horizontal or gently inclined and parallel to the shortening direction, with intermediate (σ_2) and minimum compressive stress (σ_3) axes potentially very close in magnitude but not constant in orientation through time [*Golding*, 2012]. In such a case, the shallow shear faults might be accommodating some of the tectonic shortening across the ridge. However, our data indicate that the local state of stress at shallow stratigraphic levels (<1 km depth) appears to be heterogeneous and temporally variable, with

mixed faulting styles over several kilometers and evidence of tectonic overprinting.

[32] An alternative interpretation is therefore that the regional deformation has not been purely compressive, and distributed shears (Figure 4b) may have resulted from localized partitioning of deformation under simple shear. Such deformation may reflect a transition from normal convergence near the subduction deformation front to a more mixed contractional and shear deformation regime further inboard [*Cashman et al.*, 1992; *Wallace et al.*, 2012]. Although we are not able to constrain detailed deformation beyond the area of the 3-D-seismic study, it is possible that previously unrecognized, secondary strike-slip faults are developed oblique to the ridge axis. Such faults may cut obliquely across the ridge crest and CT (Figure 4a), in a similar geometry to that observed at Uruti Ridge, 170 km to the southwest [*Barnes et al.*, 2010]. They can be active contemporaneously with the major thrust faults, and be associated with the sag basins on the ridge crest immediately east of CT (Figures 1c and 4a). We note that the orientation of inferred strike-slip faults (Figure 4a) matches that of an oblique segment of a narrow ridge between Omakere Ridge and Rock Garden, possibly indicating similar distributed shear faulting in that area (Figure 1b). In this scenario, the fault configuration at the crest of the ridge to the east of seeps Moa and Bear's Paw (i.e., extensional faults and overprinting shear faults; Figures 2a-3 and 4a) could be interpreted as a negative flower structure (Figure 5b), that formed as a kinematic response to imposed boundary constraints during the mixed contractional and shear deformation regime [e.g., *Woodcock and Fischer*, 1986].

[33] The conjugate shear faults oblique to the CT in the 3-D survey might represent some of the variety of secondary shears that form in cover sequences over strike-slip faults in simple shear models, such as Riedel R and R' shears (Figure 4b) [*Woodcock and Fischer*, 1986; *Sylvester*, 1988]. We speculate that the fact that only the NW-SE component of the conjugated fault pairs has seafloor seep sites associated (i.e., Kea, Kaka, and Kakapo seeps) is due to enhanced dilation induced by a higher proximity to σ_1. Such dilation would mean that these faults (Figure 4c) became preferential paths for funneling escaping fluids. Elongated chimneys have developed along this presumably dilated, conjugate strike-slip fault component beneath the seeps (Figure 8).

[34] Individual seep morphology at Moa and Bear's Paw sites does not reflect the orientation of
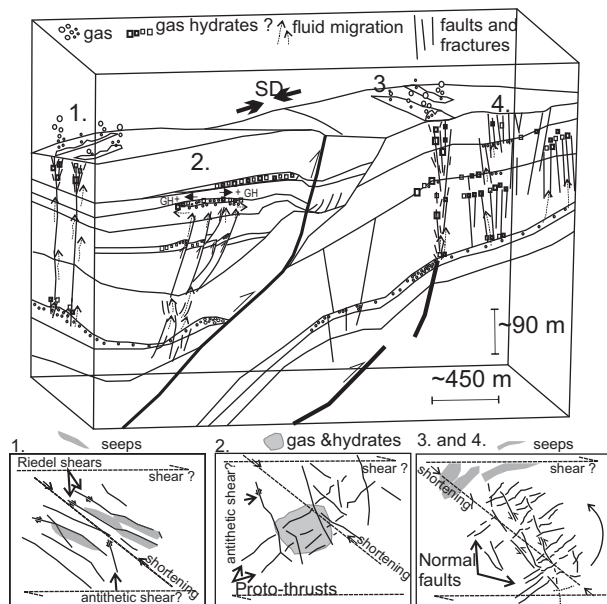
Figure 8. Conceptual model showing structures involved in four different fluid migration systems at Omakere Ridge. Small panels show the distribution of structures and inferred orientation of shortening and shear in a plan view; SD = shortening direction.

the inactive oblique shears, but rather the orientation of ridge-parallel shallowest extensional faults or thrusts (Figures 2 and 3). These seeps are related to each other, and together reflect the orientation of a major structure oriented NE-SW. We suggest that the slight clock-wise rotation of Bear's Paw with respect to Moa may be a consequence of strike-slip movement along one of the oblique curve-linear faults (Figure 4d).

[35] Although beyond the scope of this paper, our observations of shear faulting on this part of the margin will be relevant in a more regional sense for future studies of tectonic deformation processes occurring within the Hikurangi subduction margin. For example, strain partitioning along shear structures will have implications for seismic hazard assessment and for the general understanding of the tectonic setting of the plate boundary.

5.2. Fluid Migration Systems

[36] Different configurations of faults and structural traps have led to the evolution of not only fluid migration systems sustaining seafloor seepage at Omakere Ridge but also to the evolution of systems where gas-rich fluids reaccumulate laterally within the upper 300 m in the sedimentary column. We differentiate between four different fluid migration systems and refer to them numeri-

cally as: Systems 1 (the Kea, Kaka, and Kakapo seeps trio), System 2 (BR and the proto-thrusts), System 3 (Moa and Bear's Paw seeps), and System 4 (high-amplitude patches and overprinting extensional and shear faults) (Figure 8).

[37] System 1 and System 3 (Figure 8) are classic cold seep systems [e.g., *Cathles et al.*, 2010; *Talukder*, 2012]: they consist of a shallow gas accumulation zone (HAZ1 and HAZ2, respectively), a plumbing structure (i.e., chimneys), and seafloor seepage expressions (Kea, Kaka, and Kakapo in System 1; Moa and Bear's Paw in System 3). All the seeps are associated with plumbing structures comprised of more than one parallel fault and gas chimney (Figure 7b). Seafloor seepage in System 1 and System 3 can be directly linked to underlying shallow gas zones (HAZ1 and HAZ2). However, the RMS amplitude maps indicate that gas-rich zones extend beyond the zones of seafloor seepage (Figures 3d, 3e, and 7b). Each fluid migration system sustaining seafloor seepage is coupled to adjacent systems (System 2 and System 4) where gas-rich fluids migrate upward from the same source but stay trapped in the subsurface (Figure 8).

[38] System 2 and System 4 are characterized by gas-rich fluid injection through proto-thrusts and overprinting shear and extensional faults, respectively (Figure 8). Migration and redistribution of gas-rich fluids is evidenced by the exclusive location of amplitude anomalies like BR (Figure 7b) above the proto-thrusts (Figures 4a and 7b) and smaller bright reflections along fault planes at certain stratigraphic levels (Figures 3d, 3e, and 7a). The lateral decrease in RMS amplitudes recorded along TR (Figure 3d) and he300 (Figure 3e), underlying the zone of bright reflections, suggest that gas-rich fluids have migrated from the same stratigraphic level hosting HAZ1 and HAZ2 and reaccumulated in shallower stratigraphic levels or traps (Figure 3). While the observation of reverse polarity reflection along BR is consistent with the interpretation of gas bearing sediments causing the bright reflection, the shift from strong reverse polarity to moderate positive polarity toward the edge of the reflection anomaly (Figure 7b) suggests that other interpretations cannot be ruled out. BR may be indicating a zone of coexistence of free gas with high-impedance material, e.g., gas hydrates bearing sediments [e.g., *Liu and Flemings*, 2007] or buried carbonate concretions at the outer margin of the gas input zone (Figure 8). However, the only direct indication at present for gas hydrates at Omakere Ridge comes from

shallow (<3 mbsf) sediment coring [*Bialas et al.*, 2007]. Deep penetration sampling would be needed to test interpretations of gas hydrate formation or buried authigenic carbonate at the location of BR.

5.2.1. Controls on Chimney Formation and Fluid Distribution

[39] Our data show evidence for a direct control of faults on seepage distribution at Omakere Ridge, as documented for other margins [e.g., *Gay et al.*, 2007; *Hustoft et al.*, 2007; *Pilcher and Argent*, 2007]. However, the mixed contractional and shear deformation regime seems to have had a particular effect on pore-fluid pressure distribution. While increased fluid pressures in the gas-rich zones (HAZ1 and HAZ2; Figure 2) provided the driving force for fluid expulsion through faults in the four systems, fluid flow has been focused enough to form seafloor seeps and associated gas chimneys exclusively along some of the dilated components of conjugated shears in System 1 (the Kea, Kaka, and Kakapo seeps trio) and some of the extensional faults cross-crossing a blind thrust fault in System 3 (seeps Moa and Bear's Paw). Focusing versus dispersion of the flow may have been controlled by the mixed effect of stress distribution and gas-rich fluid input from depth [e.g., *Talukder*, 2012].

[40] It has been discussed whether natural hydraulic fracturing was necessary to induce the development of the gas chimneys to the present-day seafloor. Our data show that the different shear and extensional fault arrays do not extend to the seafloor (Figures 1 and 3). Moreover, several unconformities mark important changes in both the deformation regime and the seismic character of the gas chimneys (e.g., hw30-he30; Figures 2 and 5). Changes in the anatomy of chimneys and different periods of evolution have been documented e.g., for chimneys in the Norwegian margin [*Plaza-Faverola et al.*, 2011; *Gay et al.*, 2012]. These observations lead us to suggest that beneath certain stratigraphic levels, channeled fluid flow have exploited existing geological structures in order to ascend vertically but that final stages of fluid migration toward the seafloor may have occurred in the absence of large-scale, high-permeability structures. Instead, on account of lower overburden stresses at shallow depths [e.g., *Talukder*, 2012 and references therein], it is likely that the migrating fluids were able to generate their own flow paths, either by migrating in a diffusive way through sediment pore spaces or by causing hydrofracturing, which occurs when pore-fluid

pressure exceeds the minimum principal stress and the tensile strength of the sediments [*Roberts and Nunn*, 1995; *Roberts et al.*, 1996; *Luo and Vasseur*, 2002] (Figure 8). The presence of randomly distributed fractures captured on coherency maps above he30 within the chimney underlying Moa (Figure 5b) supports the notion of hydrofracturing playing a role during the latest stage of chimney development. Thus, fluid flow behaved somewhat passively, by exploiting existing structural networks at depth, and also more actively closer to the seafloor where fluids generated their own migration pathways above (and along) shear faulted weakness planes (Figure 8).

[41] Fluid flow through proto-thrusts and over-printing shear and extensional faults has been accompanied by lateral migration at different stratigraphic levels (Figures 2, 7, and 8) indicating a more disperse flow through time, likely inhibiting the formation of chimneys in these systems (Figure 8). A progressive and steady build-up of pore-fluid pressure in normally compacted sediments may have led to ductile deformation [*Bolton et al.*, 1998], inducing progressive dissipation of fluid pressure through already in-place-permeable faults. An interesting observation is the pop-up like structure that comprises System 1 (the Kea, Kaka, and Kakapo seeps) and adjacent System 2 (BR and the proto-thrusts) (Figure 7a). We interpret this structure as the result of mobilization of undercompacted-buoyant material possibly indicating pore-fluid pressures as high as lithostatic [*Behrmann*, 1991] associated with the activity of the CT. We would expect such deformation to have occurred prior to the onset of hydrofracturing and latest stages of chimney formation.

[42] While a continuous BSR (i.e., indicating the depth of the base GHSZ) is not observed in the P-Cable 3-D survey area, a 500 msbsf deep BSR is well documented in regional seismic profiles adjacent to Omakere Ridge (Figure 6). Moreover, *Krabbenhoeft et al.* [2013] and *Barnes et al.* [2010] interpret the presence of BSR indicators in 2-D seismic lines crossing the 3-D survey area. The top of the HAZ1 horizon and the flat reflections associated with it (Figure 7a) coincide with the depth of these BSR indicators [*Barnes et al.*, 2010; *Krabbenhoeft et al.*, 2013], but it appears elevated in places with respect to the projected regional BSR by up to 40 m (e.g., Figures 2a and 7a). This observation indicates, first, that free gas is not staying trapped extensively along the BGHS locally at Omakere ridge. Instead, gas may be transported away from the BGHS by fast-moving

fluids and thus BSR gaps mark areas with high rates of fluid expulsion, as postulated for other locations along this margin [*Barnes et al.*, 2010; *Pecher et al.*, 2010]. Small amounts of free gas trapped at the BGHS would be enough to form a BSR [e.g., *Bangs et al.*, 1993; *Hornbach et al.*, 2012]; and second, that shoaling of the BGHS [*Pecher et al.*, 2010; *Hornbach et al.*, 2012] is possibly occurring due to upward migration of fluids at discrete fluid injection zones (e.g., HAZ1). This could indicate that some of the fluids expelled on the Omakere Ridge originate from deep sources such as the subduction zone. Estimates of advective heat flux for the Porangahau Ridge further south, where BGHS shoaling is even more pronounced, have demonstrated that while high rates of fluid flux are required for fluids sourced from the base of the slope basins (∼1500 mbsf), only moderate flux rates are required if fluids generate at ∼5000 mbsf, the depth of the subduction interface [*Pecher et al.*, 2010].

5.3. Seepage Periodiciy

[43] Annual observations of seep sites at Omakere Ridge suggest that seepage is intermittent [*Bialas*, 2011]. This scale of intermittency may be explained by subtidal modulation of gas flows through small-scale pressure changes. However, the presence of gas hydrates and authigenic carbonate precipitations at seep sites [*Bialas*, 2011; *Golding*, 2012] suggests an auto-sealing mechanism common at methane seep sites where precipitation of authigenic carbonates [e.g., *Hovland*, 2002] or highly concentrated hydrate deposits closes off permeable flow paths to the seafloor [e.g., *Bangs et al.*, 2011; *Kannberg et al.*, 2013]. Consecutive periodes of seal-bypassing and hydrate dissosiation, followed by reaccumulation of authigenic carbonate and hydrates, respectively, leads to periodic seepage. The presence of hydrates and/or authigenic carbonate precipitations within the upper sediments beneath seeps at Omakere Ridge has been inferred based on recent analysis of backscatter and reflectivity data [*Golding*, 2012] and suggests that these auto-sealing-periodic seepage systems may have been active for many thousands of years. These interpretations are supported by the existence of reflection pull-up, especially evident in the seismic profiles beneath Kea and Kakapo (Figure 7a), which suggests an increase in seismic velocities (Figure 7c). This pull-up effect is commonly observed in chimneys piercing through the GHSZ [e.g., *Hustoft et al.*, 2007] and has been partially explained as a

velocity effect due to the acceleration of waves traveling through hard material (e.g., hydrates and/or authigenic carbonate) existing at discrete layers inside the chimneys [e.g., *Plaza-Faverola et al.*, 2010].

[44] *Jones et al.* [2010] and *Golding* [2012] suggested, based on characteristics of chemosynthetic organisms and the inferred thicknesses of authigenic carbonates, a relative chronology of the seeps with respect to each other. Moa is believed to be the seep site with the longest period of activity (part of Moa is currently inactive), while Bear's Paw is believed to be the youngest but more active seep in the region [*Jones et al.*, 2010; *Golding*, 2012]. 3-D-seismic mapping shows that the chimney associated with Bear's Paw is also the least developed among the imaged chimneys (Figure 3). Our observations support the notion of auto-sealing of Moa and lateral relocation of the gas toward Bear's Paw.

[45] At a more general scale, periodicity of seepage in marine sediments has been found to be coupled to natural fluid pressure cycles regulated by opening and closing of faults and fractures [e.g., *Rice*, 1992; *Evans et al.*, 1997; *Roberts and Carney*, 1997; *Miller and Nur*, 2000]. A recent study from offshore Pakistan demonstrates that due to the large areas affected, earthquake-triggered gas discharges to the seafloor through faults and fractures are more significant than previously suspected (i.e., with annual gas input to the oceans comparable to single mud-volcanoes in different margins) [*Fischer et al.*, 2013]. In the case of the Hikurangi margin, fluid seepage periodicity is likely to be partially coupled to earthquake cycles and fault displacement [*Hull*, 1990; *Moore and Vrolijk*, 1992; *Sibson*, 2013; *Fischer et al.*, 2013].

6. Conclusions

[46] High-resolution 3-D-seismic mapping at Omakere Ridge, offshore New Zealand's North Island, reveals shear, extensional and compressional structures implicated in gas-rich fluid migration into the gas hydrate stability zone and seafloor seepage at a scale previously not observed along the margin. Shear structures contemporaneous with major thrust faults and folds, developed at <1 km depth, under pure compression or from partitioned thrust faulting and distributed shear fracturing under simple shear. Such shear faulting has not previously been identified in this part of

the Hikurangi margin. These new observations from 3-D-seismic data will have implications for reconstructing the tectonic evolution of the Hikurangi margin, future hazards assessment and for further understanding the interaction between structural deformation and fluid expulsion along subduction margins.

[47] Complex stress heterogeneities led to the development of different fluid flow systems within an area of only 2 × 7 km. Although faults have had a direct control on fluid distribution at Omakere Ridge, the balancing effect of localized stress and fluid input from depth resulted in different styles of fluid flow through these faults (i.e., focused versus disperse), thereby determining the distribution of gas chimneys and seafloor seepage. Elevated fluid pressures in gas-rich fluid zones have provided the driving force for fluid flow through existing structural networks at depth. In the absence of pre-existing permeable paths closer to the seafloor, however, elevated pore-fluid pressures appear to actively generate fluid migration conduits by fracturing the sediments along preferential shear-faulted weakness planes. Permeable proto-thrusts and normal faults have likely facilitated progressive drainage of fluids during compaction (both, through faults and along layers), hindering chimney formation. The timing of overpressure with respect to the onset of shear and compression may be one factor determining structural differences between the fluid migration systems.

[48] The Omakere Ridge seems to be one of the key locations along the Hikurangi margin where fluids are migrating from deep sources into the hydrate zone and eventually the seafloor. Gas-rich fluid entrapment responsible for excess pore-fluid pressure generation and chimney formation has been structurally controlled and has occurred at the approximate depth of the regional base of the gas hydrate stability zone. In the absence of structural traps, gas has been transported well into the hydrate zone by deeply sourced upward migrating fluids, locally impeding the development of classic through-going BSRs.

Acknowledgments

References

Anka, Z., C. Berndt, and A. Gay (2012), Hydrocarbon leakage through focused fluid flow systems in continental margins, *Mar. Geol.*, *332–334*, 1–3, doi:10.1016/j.margeo.2012.10.012.

Bangs, N. L. B., D. S. Sawyer, and X. Golovchenko (1993), Free gas at the base of the gas hydrate zone in the vicinity of the Chile triple junction, *Geology*, *21*(10), 905–908.

Bangs, N. L. B., M. J. Hornbach, and C. Berndt (2011), The mechanics of intermittent methane venting at South Hydrate Ridge inferred from 4D seismic surveying, *Earth Planet. Sci. Lett.*, *310*(1), 105–112.

Barnes, P., A. Nicol, and T. Harrison (2002), Late Cenozoic evolution and earthquake potential of an active listric thrust complex above the Hikurangi subduction zone, New Zealand, *Geol. Soc. Am. Bull.*, *114*(11), 1379–1405.

Barnes, P., G. Lamarche, J. Bialas, S. Henrys, I. Pecher, G. L. Netzeband, J. Greinert, J. J. Mountjoy, K. Pedley, and G. Crutchley (2010), Tectonic and geological framework for gas hydrates and cold seeps on the Hikurangi subduction margin, New Zealand, *Mar. Geol.*, *272*(1), 26–48.

Beavan, J., P. Tregoning, M. Bevis, T. Kato, and C. Meertens (2002), Motion and rigidity of the Pacific Plate and implications for plate boundary deformation, *J. Geophys. Res.*, *107*(B10), 2261, doi:10.1029/2001JB000282.

Behrmann, J. (1991), Conditions for hydrofracture and the fluid permeability of accretionary wedges, *Earth Planet. Sci. Lett.*, *107*(3–4), 550–558.

Berndt, C., S. Bünz, and J. Mienert (2003), Polygonal fault systems on the mid-Norwegian margin: A long-term source for fluid flow, *Geol. Soc. Spec. Publ.*, *216*(1), 283–290.

Berndt, C., S. Costa, M. Canals, A. Camerlenghi, B. de Mol, and M. Saunders (2012), Repeated slope failure linked to fluid migration: The Ana submarine landslide complex, Eivissa Channel, Western Mediterranean Sea, *Earth Planet. Sci. Lett.*, *319*, 65–74.

Berryman, K., and S. Beanland (1988), Ongoing deformation of New Zealand: Rates of tectonic movement from geological evidence, *Trans. Inst. Prof. Eng. N. Z.*, *15*(1), 25–35.

Bialas, J. (2011), *FS SONNE Fahrtbericht/Cruise report SO214 NEMESYS: 09.03.−05.04. 2011, Wellington-Wellington, 06.−22.04. 2011*, Wellington-Auckland.

Bialas, J., J. Greinert, P. Linke, and O. Pfannkuche (2007), *RV Sonne Fahrtbericht/Cruise Rep. SO 191-New Vents "Puaretanga Hou": Wellington-Napier-Auckland, 11.01.−23.03. 2007*.

Bolton, A., A. Maltman, and M. Clennell (1998), The importance of overpressure timing and permeability evolution in fine-grained sediments undergoing shear, *J. Struct. Geol.*, *20*(8), 1013–1022.

Bünz, S., J. Mienert, M. Vanneste, and K. Andreassen (2005), Gas hydrates at the Storegga Slide: Constraints from an analysis of multicomponent, wide-angle seismic data, *Geophysics*, *70*(5), B19–B34, doi:10.1190/1.2073887.

Cartwright, J. (2011), Diagenetically induced shear failure of fine-grained sediments and the development of polygonal fault systems, *Mar. Petrol. Geol.*, 28(9), 1593–1610, doi: 10.1016/j.marpetgeo.2011.06.004.

Cartwright, J., M. Huuse, and A. Aplin (2007), Seal bypass systems, *AAPG Bull.*, 91(8), 1141–1166.

Cashman, S. M., H. M. Kelsey, C. F. Erdman, H. N. C. Cutten, and K. R. Berryman (1992), Strain partitioning between structural domains in the forearc of the Hikurangi subduction zone, New Zealand, *Tectonics*, 11(2), 242–257.

Cathles, L. M., Z. Su, and D. Chen (2010), The physics of gas chimney and pockmark formation, with implications for assessment of seafloor hazards and gas sequestration, *Mar. Petrol. Geol.*, 27(1), 82–91.

Cole, J., and K. Lewis (1981), Evolution of the Taupo-Hikurangi subduction system, *Tectonophysics*, 72(1–2), 1–21.

Collot, J. Y., J. Delteil, K. B. Lewis, B. Davy, G. Lamarche, J. C. Audru, P. Barnes, F. Chanier, E. Chaumillon, and S. Lallemand (1996), From oblique subduction to intra-continental transpression: Structures of the southern Kermadec-Hikurangi margin from multibeam bathymetry, side-scan sonar and seismic reflection, *Mar. Geophys. Res.*, 18, 357–381.

Crutchley, G. J., A. R. Gorman, I. A. Pecher, S. Toulmin, and S. A. Henrys (2011), Geological controls on focused fluid flow through the gas hydrate stability zone on the southern Hikurangi Margin of New Zealand, evidenced from multichannel seismic data, *Mar. Petrol. Geol.*, 28(10), 1915–1931.

Davey, F. J., M. Hampton, J. Childs, M. A. Fisher, K. Lewis, and J. R. Pettinga (1986), Structure of a growing accretionary prism, Hikurangi margin, New Zealand, *Geology*, 14(8), 663–666.

Denman, K. L., G. Brasseur, A. Chidthaisong, P. Ciais, P. M. Cox, R. E. Dickinson, D. Hauglustaine, C. Heinze, E. Holland, and D. Jacob (2007), Couplings between changes in the climate system and biogeochemistry, *Clim. Change*, 2007, 541–584.

Dickens, G. R., J. R. O'Neil, D. K. Rea, and R. M. Owen (1995), Dissociation of oceanic methane hydrate as a cause of the carbon isotope excursion at the end of the Paleocene, *Paleoceanography*, 10, 965–971.

Etiope, G. (2009), Natural emissions of methane from geological seepage in Europe, *Atmos. Environ.*, 43(7), 1430–1443.

Etiope, G., K. R. Lassey, R. W. Klusman, and E. Boschi (2008), Reappraisal of the fossil methane budget and related emission from geologic sources, *Geophys. Res. Lett.*, 35(9), L09307, doi:10.1029/2008gl033623.

Evans, J. P., C. B. Forster, and J. V. Goddard (1997), Permeability of fault-related rocks, and implications for hydraulic structure of fault zones, *J. Struct. Geol.*, 19(11), 1393–1404.

Faure, K., J. Greinert, J. S. von Deimling, D. F. McGinnis, R. Kipfer, and P. Linke (2010), Methane seepage along the Hikurangi Margin of New Zealand: Geochemical and physical data from the water column, sea surface and atmosphere, *Mar. Geol.*, 272(1–4), 170–188.

Fischer, D., J. M. Mogollon, M. Strasser, T. Pape, G. Bohrmann, N. Fekete, V. Spiess, and S. Kasten (2013), Subduction zone earthquake as potential trigger of submarine hydrocarbon seepage, *Nat. Geosci*, 6(8), 647–651, doi: 10.1038/ngeo1886, [Available at http://www.nature.com/ngeo/journal/v6/n8/abs/ngeo1886.html#supplementary-information.].

Gay, A., M. Lopez, C. Berndt, and M. Seranne (2007), Geological controls on focused fluid flow associated with sea-floor seeps in the Lower Congo Basin, *Mar. Geol.*, 244, 68–92, doi:10.1016/j.margeo.2007.06.003.

Gay, A., R. Mourgues, C. Berndt, D. Bureau, S. Planke, D. Laurent, S. Gautier, C. Lauer, and D. Loggia (2012), Anatomy of a fluid pipe in the Norway Basin: Initiation, propagation and 3D shape, *Mar. Geol.*, 332–334, 75–88, doi: 10.1016/j.margeo.2012.08.010.

Golding, T. (2012), *A multi-frequency acoustic investigation of seafloor methane seep sites at Omakere Ridge, Hikurangi Margin, New Zealand, Masters thesis*, 114 pp., Victoria Univ. of Wellington, Wellington.

Greinert, J., K. B. Lewis, J. Bialas, I. A. Pecher, A. Rowden, D. A. Bowden, M. De Batist, and P. Linke (2010), Methane seepage along the Hikurangi Margin, New Zealand: Overview of studies in 2006 and 2007 and new evidence from visual, bathymetric and hydroacoustic investigations, *Mar. Geol.*, 272(1–4), 6–25.

Haines, A. J., and D. Darby (1987), *Preliminary Dislocation Models for the 1931 Napier and 1932 Wairoa Earthquakes*, N. Z. Geol. Surv. Rep., Dept. of Sci. and Ind. Res., Lower Hutt, New Zealand.

Hamilton, E. L. (1978), Sound velocity–density relations in seafloor sediments and rocks, *J. Acoust. Soc. Am.*, 63(2), 366–377, doi:10.1121/1.381747.

Hornbach, M. J., N. L. Bangs, and C. Berndt (2012), Detecting hydrate and fluid flow from bottom simulating reflector depth anomalies, *Geology*, 40(3), 227–230.

Hovland, M. (2002), On the self-sealing nature of marine seeps, *Cont. Shelf Res.*, 22(16), 2387–2394.

Hull, A. G. (1990), Tectonics of the 1931 Hawke's Bay earthquake, *N. Z. J. Geol. Geophys.*, 33(2), 309–320.

Hustoft, S., J. Mienert, S. Bünz, and H. Nouzé (2007), High-resolution 3D-seismic data indicate focussed fluid migration pathways above polygonal fault systems of the mid-Norwegian margin, *Mar. Geol.*, 245(1–4), 89–106.

Hustoft, S., S. Bünz, and J. Mienert (2010), Three-dimensional seismic analysis of the morphology and spatial distribution of chimneys beneath the Nyegga pockmark field, offshore mid-Norway, *Basin Res.*, 22(4), 465–480.

Hyndman, R. D., and E. E. Davis (1992), A mechanism for the formation of methane hydrate and seafloor bottom-simulating reflectors by vertical fluid expulsion, *J. Geophys. Res.*, 97(B5), 7025–7041.

Jones, A. T., J. Greinert, D. Bowden, I. Klaucke, C. J. Petersen, G. Netzeband, and W. Weinrebe (2010), Acoustic and visual characterisation of methane-rich seabed seeps at Omakere Ridge on the Hikurangi Margin, *New Zealand*, Mar. Geol., 272(1), 154–169.

Judd, A. G., and M. Hovland (2007), *Seabed Fluid Flow: The Impact of Geology, Biology and the Marine Environment*, 475 pp., Cambridge Univ. Press, Cambridge.

Kannberg, P. K., A. M. Tréhu, S. D. Pierce, C. K. Paull, and D. W. Caress (2013), Temporal variation of methane flares in the ocean above Hydrate Ridge, Oregon, *Earth Planet. Sci. Lett.*, 368, 33–42.

Kennett, J. P., K. G. Cannariato, I. L. Hendy, and R. J. Behl (2003), *Methane Hydrates in Quaternary Climate Change: The Clathrate Gun Hypothesis*, 216 pp., AGU, Washington, D. C.

Krabbenhoeft, A., J. Bialas, I. Klaucke, G. Crutchley, C. Papenberg, and G. L. Netzeband (2013), Patterns of subsurface fluid-flow at cold seeps: The Hikurangi Margin, offshore New Zealand, *Mar. Petrol. Geol.*, 39(1), 59–73.

Kroeger, K. F., R. Di Primio, and B. Horsfield (2011), Atmospheric methane from organic carbon mobilization in

sedimentary basins – The sleeping giant?, *Earth Sci. Rev.*, *107*(3), 423–442.

Kurtz, A., L. Kump, M. Arthur, J. Zachos, and A. Paytan (2003), Early Cenozoic decoupling of the global carbon and sulfur cycles, *Paleoceanography*, *18*(4), 1090, doi:10.1029/2003PA000908.

Kvenvolden, K. A. (2002), Methane hydrate in the global organic carbon cycle, *Terra Nova*, *14*(5), 302–306.

Lewis, K. B., and J. R. Pettinga (1993), *The emerging, imbricate frontal wedge of the Hikurangi margin, in South Pacific Sedimentary Basins. Sedimentary Basins of the World*, vol. *2*, edited by P. F. Ballance, pp. 225–250, Elsevier, New York.

Liu, X. L., and P. B. Flemings (2007), Dynamic multiphase flow model of hydrate formation in marine sediments, *J. Geophys. Res.*, *112*(B3), B03101, doi:10.1029/2005jb004227.

Løseth, H., M. Gading, and L. Wensaas (2009), Hydrocarbon leakage interpreted on seismic data, *Mar. Petrol. Geol.*, *26*(7), 1304–1319, doi:10.1016/j.marpetgeo.2008.09.008.

Luo, X., and G. Vasseur (2002), Natural hydraulic cracking: Numerical model and sensitivity study, *Earth Planet. Sci. Lett.*, *201*(2), 431–446.

MacDonald, G. J. (1990), Role of methane clathrates in past and future climates, *Clim. Change*, *16*(3), 247–281.

Milkov, A. V., R. Sassen, T. V. Apanasovich, and F. G. Dadashev (2003), Global gas flux from mud volcanoes: A significant source of fossil methane in the atmosphere and the ocean, *Geophys. Res. Lett.*, *30*(2), 1037, doi:10.1029/2002GL016358.

Miller, S. A., and A. Nur (2000), Permeability as a toggle switch in fluid-controlled crustal processes, *Earth Planet. Sci. Lett.*, *183*(1), 133–146.

Moore, J. C., and P. Vrolijk (1992), Fluids in accretionary prisms, *Rev. Geophys.*, *30*(2), 113–135.

Netzeband, G. L., C. P. Hübscher, D. Gajewski, J. W. G. Grobys, and J. Bialas (2005), Seismic velocities from the Yaquina forearc basin off Peru: Evidence for free gas within the gas hydrate stability zone, *Int. J. Earth Sci.*, *94*(3), 420–432.

Paquet, F., J.-N. Proust, P. M. Barnes, and J. R. Pettinga (2011), Controls on active forearc basin stratigraphy and sediment fluxes: The Pleistocene of Hawke Bay, New Zealand, *Geol. Soc. Am. Bull.*, *123*(5–6), 1074–1096.

Pecher, I. A., S. A. Henrys, W. T. Wood, N. Kukowski, G. J. Crutchley, M. Fohrmann, J. Kilner, K. Senger, A. R. Gorman, and R. B. Coffin (2010), Focussed fluid flow on the Hikurangi Margin, New Zealand – Evidence from possible local upwarping of the base of gas hydrate stability, *Mar. Geol.*, *272*(1–4), 99–113.

Pilcher, R., and J. Argent (2007), Mega-pockmarks and linear pockmark trains on the West African continental margin, *Mar. Geol.*, *244*(1–4), 15–32.

Planke, S., and C. Berndt (2003), Apparatus for seismic measurements, Norwegian Patent [317652].

Plaza-Faverola, A., G. K. Westbrook, S. Ker, R. Exley, A. Gailler, T. A. Minshull, and K. Broto (2010), Evidence from three-dimensional seismic tomography for a substantial accumulation of gas hydrate in a fluid-escape chimney in the Nyegga pockmark field, offshore Norway, *J. Geophys. Res*, *115*, B08104, doi:10.1029/2009JB007078.

Plaza-Faverola, A., S. Bünz, and J. Mienert (2011), Repeated fluid expulsion through sub-seabed chimneys offshore Norway in response to glacial cycles, *Earth Planet. Sci. Lett.*, *305*(3–4), 297–308, doi:10.1016/j.epsl.2011.03.001.

Rice, J. R. (1992), Fault stress states, pore pressure distributions, and the weakness of the San Andreas fault, *Int. Geophys. Ser.*, *51*, 475–475.

Roberts, H. H., and R. S. Carney (1997), Evidence of episodic fluid, gas, and sediment venting on the northern Gulf of Mexico continental slope, *Econ. Geol.*, *92*(7–8), 863–879.

Roberts, S. J., and J. Nunn (1995), Episodic fluid expulsion from geopressured sediments, *Mar. Petrol. Geol.*, *12*(2), 195–204.

Roberts, S. J., J. Nunn, L. M. Cathles, and F. Cipriani (1996), Expulsion of abnormally pressured fluids along faults, *J. Geophys. Res.*, *101*(B12), 28,231–28,228, 28252.

Sibson, R. H. (2013), Stress switching in subduction forearcs: Implications for overpressure containment and strength cycling on megathrusts, *Tectonophysics*, *600*(0), 142–152, doi:10.1016/j.tecto.2013.02.035.

Svensen, H. (2012), Geochemistry: Bubbles from the deep, *Nature*, *483*(7390), 413–415.

Sylvester, A. G. (1988), Strike-slip faults, *Geol. Soc. Am. Bull.*, *100*(11), 1666–1703.

Talukder, A. R. (2012), Review of submarine cold seep plumbing systems: Leakage to seepage and venting, *Terra Nova*, *24*(4), 255–272.

Wallace, L., J. Beavan, R. McCaffrey, and D. Darby (2004), Subduction zone coupling and tectonic block rotations in the North Island, New Zealand, *J. Geophys. Res.*, *109*(12), 1–21.

Wallace, L., P. Barnes, J. Beavan, R. Van Dissen, N. Litchfield, J. Mountjoy, R. Langridge, G. Lamarche, and N. Pondard (2012), The kinematics of a transition from subduction to strike-slip: An example from the central New Zealand plate boundary, *J. Geophys. Res.*, *117*(B2), B02405, doi:10.1029/2011JB008640.

Woodcock, N. H., and M. Fischer (1986), Strike-slip duplexes, *J. Struct. Geol.*, *8*(7), 725–735.

Zühlsdorff, L., and V. Spiess (2004), Three-dimensional seismic characterization of a venting site reveals compelling indications of natural hydraulic fracturing, *Geology*, *32*(2), 101–104.